[Steps For Civil, Constructions and Environmental Engineering (SCCEE)](#)
ISSN: 3005-8198 (online) / 3005-818X (print)
Volume 4, Issue 2 (April – June 2026), pp: 1-13

Research Article

Use ACI Standards and Reviews Equations to Determine the Primary Parameters for the Design Reinforced Shear and 3D-Printed Concrete Walls

Salhah A. Mohummed [a*], Hana Abdalftah Aljewifi [b]

Laboratory of building materials, Civil engineering department, Omar AlMukhtar University, Elbeida, Libya.

E-mail: lalyabdo1033@gmail.com [a,*], hana.aljewifi@omu.edu.ly [b]

Received: 17 September 2025 | Revised: 02 January 2026 | Accepted: 23 March 2026 | Published: 14 April 2026

Abstract

In the domain of construction, the practice of virtual fabrication, which encompasses the utilization of three-dimensional printers in the fabrication of building components, is experiencing a notable surge in popularity and adoption. The implementation of these building strategies offers a range of advantages, including the potential for free form architecture, reduced construction time, labor expenses, waste material, and freedom of geometry. In the wet manufacturing method known as 3D Printing Concrete (3DCP), layers of extruded mortar are linked together by consecutive material deposition. The objective of this study is to make a comparison between the numerical values derived from equation reviews of ordinary reinforced shear concrete walls (RSCW) and 3D-printed concrete walls (3DPCW). Additionally, the rheological behavior and engineering mechanisms of two buildings at both the fresh and hardened states will be examined. The study assesses critical parameters, including yield stress τ_0, plastic viscosity μ_0, and the thixotropic structuration rate A_{0hix}. The findings of the study demonstrate that conventional concrete demonstrates a substantially elevated structuration rate, $A_{thix}\approx 1.14$ Pa/s, in comparison to that of 3D-printed mortar, $A_{thix}\approx 0.75$ Pa/s. While the higher rate in conventional concrete facilitates a rapid reduction in lateral formwork pressure, it concomitantly narrows the interlayer bonding window, thereby increasing the risk of cold joints. The analysis confirms that both materials exhibit viscoplastic behavior, transitioning from a solid-like state to a fluid-like response upon exceeding the yield threshold. Moreover, the findings indicate that a 20% increase in material density necessitates a 15% reduction in printing velocity to prevent plastic collapse or elastic buckling. Furthermore, the structural stability of 3DPC is constrained by an $A_{thix}/\dot{H}$ ratio > 1 s/m and a density threshold of <2,200 kg/m³. These findings establish a quantitative "safe printing envelope" for transitioning from conventional reinforced construction to automated additive manufacturing.

Keywords: *3D Printed Concrete Wall; Shear Wall; Fresh Properties; Hardened Properties; Numerical Study.*

*** Correspondence Author**

Cite This Article: Mohummed, S. A., & Aljewifi, H. A. (2026). Use ACI Standards and Reviews Equations to Determine the Primary Parameters for the Design Reinforced Shear and 3D-Printed Concrete Walls. *Steps For Civil, Constructions and Environmental Engineering*, *4*(2), 1-13. https://doi.org/10.61706/sccee12011232

Introduction

The construction industry has undergone a radical transformation since the 1980s, largely due to the emergence of additive manufacturing technologies, particularly 3D Concrete Printing (3DCP). This technology signifies a paradigm shift from conventional casting methods, wherein materials are deposited layer-by-layer based on a digital model, typically initiated from a Standard Tessellation Language (STL) format (ISO/ASTM 52900:2021(en), 2021). This digital transition has been shown to enhance stakeholder interaction, leading to a reduction in human error and an improvement in construction quality (Hernández Vargas, 2023). The adoption of 3DCP is justified by its promise of architectural freedom, waste reduction, process automation, and increased efficiency (ISO/ASTM 52900:2021(en), 2021).

The significance of 3DCP stems from its capacity to address the global housing crisis and the construction industry's suboptimal productivity levels. The elimination of formwork, a conventionally necessary component of concrete construction accounting for 50% to 90% of costs, is a primary benefit. Additionally, the ability to generate complex, topology-optimized geometries while utilizing material sparingly and only where structural necessity demands it, represents a significant advancement. However, it must be acknowledged that the technology is not without its disadvantages. The contemporary challenges associated with this field include the necessity of elevated cement content in printable mixtures, which has the potential to augment the initial carbon footprint per unit volume. Additionally, the inherent anisotropy of printed components, wherein the interfaces between layers function as "weak links" in structural integrity, is a salient concern. Additionally, the absence of standardized reinforcement methods constitutes a substantial impediment to the widespread adoption of these structures. While the current driver is linked to productivity, its most significant contribution lies in manufacturing material-efficient structures by integrating structural analysis directly into the design process (Hernández Vargas, 2023).

The conceptual underpinnings of printable construction can be traced back to the late 1990s, with initial research concentrating on substantiating the viability of the approach through the utilization of rudimentary cementitious materials (Bos et al., 2016). However, the true evolution of this technology began with parallel advancements in robotics and material science, enabling the printing of structural-scale elements (Buchanan & Gardner, 2019). Modern 3DCP systems are generally categorized by their manipulators, predominantly industrial robotic arms which offer high degrees of freedom (DOF) for intricate designs, or gantry systems favored for large-scale on-site applications (Hernández Vargas, 2023). This technological advancement has led to its increased adoption in real-world projects (Khoshnevis, 2004). Notable applications include the Striatus Bridge in Venice, an unreinforced masonry-style arch composed of 53 3DCP blocks, and the Milestone Project in Eindhoven, which produced the first 3D-printed inhabited home. Among the most recent state-of-the-art applications is the 3dpod by Obayashi Corporation (2023), the first 3D-printed building to receive full certification under Japan's rigorous building standards, utilizing high-strength steel-fiber-reinforced concrete (Hernández Vargas, 2023). However, the transition to 3DCP introduces substantial rheological and structural challenges. Conventional concrete is designed to ensure flowability in formworks; however, printable concrete must possess a delicate balance of extrudability, pumpability, and buildability (Kruger et al., 2019). Typically, mixes incorporate additives such as superplasticizers and viscosity-modifying agents to achieve the required characteristics (Le, Austin, Lim, Buswell, Gibb, et al., 2012). The rheological behavior is commonly described using constitutive models like the Bingham or Herschel–Bulkley models. In these models, yield stress (τ0), plastic viscosity (μn), and thixotropic structuration rate (Athix) are considered critical descriptors (Le, Austin, Lim, Buswell, Law, et al., 2012). In the Bingham model, fresh concrete is assumed to remain an elastic solid until a critical shear stress is reached. Once this threshold is exceeded, the material transitions to a viscous fluid state (Hernández Vargas, 2023). Additionally, the Bingham model underestimates flow resistance by approximately 30%, while the Herschel–Bulkley model more accurately reflects the distinct anisotropy and shear-thinning characteristics of 3D-printed concrete (Wallevik, 2003). In order to maintain the stability of stacked layers, the material must initially exhibit fluid-like behavior and subsequently rapidly transition into a solid-like state (Ma et al., 2018). The nozzle size plays a pivotal role in regulating the material's velocity and stress condition, directly impacting its capacity to become a self-supporting structure (Mechtcherine et al., 2019). In this state, failures are generally classified into two categories: plastic collapse, defined as the occurrence of failure when the self-weight exceeds the material's yield stress, and elastic buckling, a stability-related failure that arises as the structure undergoes growth (Hernández Vargas, 2023). As indicated in the extant literature, the time of collapse corresponds to the moment when the applied building stress becomes equal to the material's shear strength, which increases over time due to thixotropic structuration (Kruger et al., 2019). Upon undergoing a phase transition, the printed material exhibits viscoplastic behavior, transitioning from a solid-like to a fluid-like response beyond its yield threshold (Perrot et al., 2016). The final shear strength and resistance to buckling are further impacted by porosity and bond strength at the interlayer interfaces. The final hardened state is characterized by the following factors: The design of safe buildings necessitates meticulous consideration of the critical collapse height and interlayer shear resistance (Van Der Putten et al., 2019). To comprehend these intricate phenomena, numerical application has become an indispensable tool, providing insights that are difficult to obtain without physical testing (Wolfs et al., 2019). A direct comparison of the early-age structural stability mechanisms between reinforced shear concrete walls (RSCW) and 3D-printed reinforced concrete walls (3DPCW) remains a significant research gap, despite the advancements in the field. The present work is contingent upon the context, as evidenced by the employment of numerical equations from reviews to draw parallels between the two systems. The former system is referred to as reinforced shear concrete walls (RSCW) as delineated by ACI Committee 318 in 2014, while the latter is designated as 3D-printed reinforced concrete walls (3DPCW), as defined by TMS 402/602 (Masonry Standards Joint Committee, 2013). A comprehensive calculation and analysis of all governing parameters has been conducted at both the fresh and hardened states. These parameters include, but are not limited to, viscosity, structuration rate, interlayer bonding, shear strength, critical height, and failure limits. In contrast to previous research, this study directly compares both systems to identify the "safe printing zone," which is defined as the precise balance where printing speed must match the material's hardening rate. Furthermore, it substantiates the indispensability of the Herschel–Bulkley model in averting the underestimation of the stability of 3D-printed structures.

Literature Review

The transition from reinforced shear concrete walls (RSCW) to 3D-printed concrete (3DPCW) signifies a paradigm shift in the field of structural engineering. Conventional systems rely on external formwork for stability, whereas 3DPC relies on the material evolving mechanically in real-time to support its own weight.

Reinforced Shear Concrete Wall (RSCW)

Conventional RSCW analysis is chiefly concerned with long-term structural capacity, frequently neglecting the intricate rheological demands of the fresh state.

Fresh State Properties

Fresh concrete is a thixotropic viscoplastic suspension. A notable limitation in earlier studies was the assumption of constant yield stress; however, recent research demonstrates that yield stress τ_0 increases linearly during rest due to physical flocculation (Banfill, 1991; Ferraris, 1999; Kosmatka & Wilson, 2011; Mehta & Monteiro, 2014; Mindess et al., 2003; Neville, 2012).

$$\tau_0(t) = \tau_0 + A_{thix} * t \quad (1)$$

In this model, $Athix$ is defined as the structuration rate. As posited by Roussel (2006), high thixotropy is imperative in minimizing lateral formwork pressure and thereby stabilizing the internal structure. This relationship is encapsulated by the following equation:

$$\tau = (1 + \lambda)\tau_0 + \mu_p\dot{\gamma} \quad (2)$$

The critical bonding interval between layers, designated as Δt_c, is determined by the rate of stiffening to prevent cold joints (Roussel, 2006).

$$\Delta t_c = \frac{\mu_p\dot{\gamma}}{A_{thix}h} \quad (3)$$

It has been demonstrated that stronger thixotropy (higher A_{thix}) results in accelerated stiffening and reduced bonding intervals. The Bingham model, which describes the viscoplastic flow of materials, is outlined as follows (ACI Committee 238, 2008; Tattersall & Banfill, 1983):

$$\tau = \tau_0 + \mu_p\dot{\gamma} \quad (4)$$

While extant studies have established the linear growth of yield stress, they often fail to quantify how this rate directly competes with the deposition speed in a comparative framework with 3D printing, a gap this study aims to bridge.

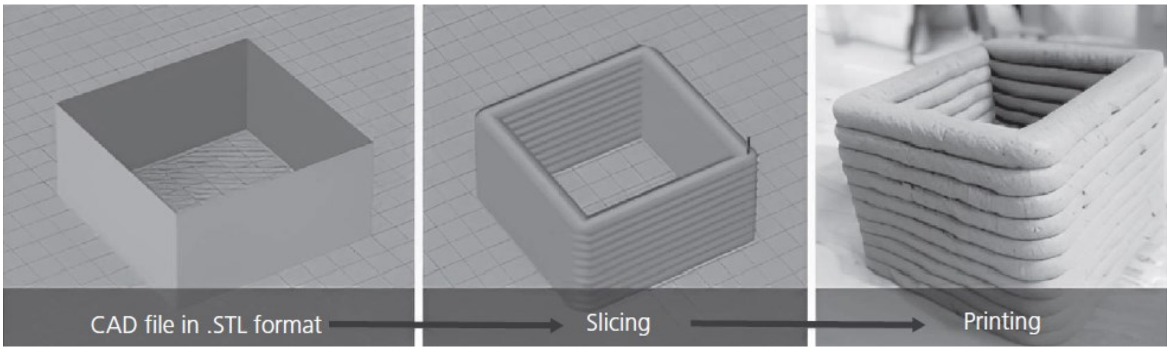

Figure 1. Workflow of 3D Concrete Printing from Digital Model to Physical Object (Panda et al., 2024).

Table 1. List of Abbreviations and Notations.

Symbol	Parameter Description
τ_0 (t)	Time-dependent yield stress.
K	Herschel Bulkley consistency (Pa.s^n).
$\dot{\gamma}$	The shear rate (s^{-1}).
n	The flow index.
μ	The viscosity (Pa.s).
τ	Shear stress (Pa).
A_{thix}	Structuring rate (Pa/s).
t	The duration of the rest period (s).
L	The length of the pipe (m).
v_b	Nozzle movement speed in the XY plane (m/s).
h_0	Height of a deposited layer (m).
ρ	Density (kg/m³).
g	The gravitational constant (m/s²).
$\dot{H}$	Layer rise speed (m/s).
v_e	Extrusion speed (m/s).
v_z	Nozzle movement speed along the Z axis (m/s).
Qe	Extrusion flow rate (m³/s).
S_b	Cross-sectional area of the nozzle (m^2).
$H_{c,e}$	Critical height of the printed object (m).
$H(t)$	Height of the printed object at time t (m).
σ_v	The vertical stress (Pa).
σc (t)	Compressive resistance.
α_{geom}	Geometric factor.
tf	Instant of crushing failure (s).
$H_{c,f}$	Critical height of the printed object leading to buckling (m).
E	Young's modulus (Pa).
α	Breakdown coefficient.
λ	structural parameter (Degree of structure), $0 \le \lambda \le 1$.
$\dot{\gamma}$	Shear rate during extrusion (s^{-1}).
μ_p or ηpl	Plastic viscosity.
Δt_c	Is the time after which the two layers will not mix (s).
S	The section of the structure printed in a horizontal plane (m^2).

Hardened State Properties

To describe the behavior of the traditional shear wall, researchers have followed established viscoplastic solid models (ACI Committee 238, 2008; Tattersall & Banfill, 1983). Upon surpassing the yield threshold, the material undergoes a transition from a solid-like to a flow-like behavior, which can be modeled by the Herschel-Bulkley law.

$$\tau = \tau_0 + K\dot{\gamma}^n, \dot{\gamma} = 0 \quad \text{for } \tau < \tau_B \qquad (5)$$

A limitation identified in previous studies (ACI Committee 238, 2008) is the insufficient analysis of energy dissipation during the plastic transition, which is defined as:

$$P = \tau\,\dot{\gamma} \qquad (6)$$

Viscoplastic models that are currently in use offer a steady-state description; however, they lack the parametric sensitivity analysis necessary to predict the transitionary failure modes that occur when switching from formwork to free-standing layers.

3D Printed Concrete Walls (3DPCW)

This section is chiefly concerned with the legal framework and conceptual underpinnings of behavior (Benamara, 2021). However, the formwork-free nature of 3DPC necessitates a shift from conventional rheological constraints (formwork pressure) to new mechanical requirements (buildability and early-age stability), requiring the application of solid mechanics models.

Fresh State Properties

A critical limitation of early 3DPC research was the failure to account for the rapid rheological transition required for formwork-free construction. The material under consideration must function as a pumpable paste while simultaneously acting as a self-supporting solid upon deposition. The phenomenon is governed by the principle of thixotropy, which refers to the reversible microstructural breakdown that occurs under shear and subsequent recovery at rest. For brief periods of rest, the yield stress (τ_0) evolution is commonly assumed to be linear (Benamara, 2021).

$$\tau_0(t) = \tau_0(0) + A_{thix} * t \quad (7)$$

In the context of rheological analysis, the term "τ_0 (0)" denotes the initial yield stress following a mixing process, while A_{thix} (Pa/s) represents the structuration (reflocculation) rate. The optimal printing speed is directly proportional to the degree of thixotropic recovery. The maximum horizontal nozzle velocity (vb) that allows for the avoidance of collapse is as follows (Benamara, 2021):

$$v_b < \sqrt{3} \cdot L \cdot A_{thix} / (\rho g\, h_0) \quad (8)$$

The material density is denoted by ρ, the gravitational constant is denoted by g, the printed length is denoted by L, and the layer height is denoted by h_0. The vertical build rate is contingent upon the horizontal speed (v_b) and the nozzle rise velocity (v_z).

$$\dot{H} = \frac{h0}{\frac{L}{vb} + \frac{h0}{Vz}} \quad (9)$$

In order to ensure the continuous and defect-free extrusion process, it is imperative that the extrusion velocity (v_e) be equivalent to the nozzle motion.

$$v_e = \frac{Qe}{Sb} \approx v_b \quad (10)$$

Therefore, the quality of the printed product is contingent upon achieving an equilibrium between rheological buildup and deposition kinematics. The utilization of additives, such as viscosity-modifying agents, serves to mitigate drainage and ensure consistent extrusion. The prevailing literature in this field treats these parameters in isolation; however, the limitation lies in the lack of a unified "safe printing envelope" that correlates material density with nozzle kinematics, which is a primary focus of this numerical investigation.

Hardened State Properties

Subsequent layers must be able to withstand the weight of the deposited material without deformation. Concrete is commonly regarded as a simple fluid; however, within the framework of 3DPC, it manifests as a viscoplastic solid, governed by the Herschel–Bulkley constitutive law (Benamara, 2021).

$$T = K\,\dot{\gamma}^n + \tau_0 \quad (11)$$

In the context of practical construction-scale applications, the simplified Bingham form (n=1) is frequently analyzed.

$$T = \tau_0 + \mu\dot{\gamma} \quad (12)$$

As illustrated in Figure 2, the shear stress versus shear rate relationship can be categorized into two models: the Bingham and the Herschel–Bulkley models.

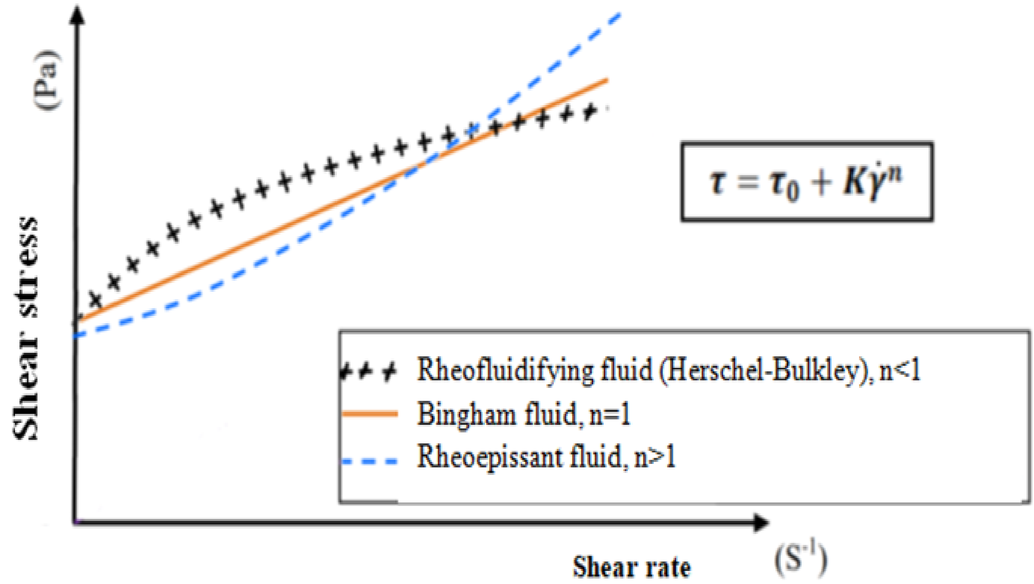

Figure 2. Illustration of the Evolution of the Shear Stress as a Function of the Shear Gradient for a Bingham Fluid (Linear Relationship Traced Continuously for n = 1) and Two Complex Fluids of the Herschel-Bulkley Model with Flow Indices n Less Than 1 (Benamara, 2021).

Critical Failure Mechanisms

It is evident that previous studies have frequently fallen short in distinguishing between the two primary modes of structural collapse that occur during the printing process. The phenomenon of crushing and buckling is of particular interest in this study.

1. Crushing Failure: This phenomenon occurs when the accumulated load surpasses the time-

dependent yield stress of the base layer. The critical height $H_{c,e}$ is defined as:

$$H_{c,e} = \frac{\sqrt{3}\tau_0(t)}{\rho g} \tag{13}$$

Where the vertical stress on the base layer σ_v is:

$$\sigma_v = \rho g H(t) = \rho g \dot{H} t \tag{14}$$

And the compressive resistance σ_c evolves according to:

$$\sigma_c(t) = \alpha_{geom} \cdot \tau_0(t) \tag{15}$$

The failure time tf then results from:

$$tf = \frac{\tau_0}{\frac{\rho g \dot{H}}{\alpha geom} - A_{thix}} \tag{16}$$

2. Buckling failure: In the case of slender structures, the predominant instability is that of elastic instability. The critical buckling height $H_{c,f}$ exhibits a cubic-root relationship with the time-dependent elastic modulus E(t):

$$H_{c,f} = \left(\frac{8EI}{\rho g S}\right)^{1/3} \tag{17}$$

The cubic-root relationship indicates that enhancing stiffness, denoted by E', contributes to improved stability, albeit with diminishing returns. This underscores the interplay between material evolution and geometric accuracy in ensuring printing stability and layer integrity (Benamara, 2021).

Application Numerical and Discussions

The theoretical framework is evaluated numerically using the parameters from Tables 2 and 3. A parametric study is conducted, in which the material density is varied to assess its specific effect on layer stability and structural resistance. The findings from this analysis are presented and interpreted in the following discussion.

Table 2. Parameters of Shear Wall at Fresh State.

Symbol	Typical Value/Unit	Notes/ References
τ_0	1200 Pa	(Banfill, 1991; Ferraris, 1999)
μ_p or η_{pl}	600	(Banfill, 1991; Ferraris, 1999)
K, n	K = 10 Pa·s^n, n = 0.5 (shear-thinning)	(Banfill, 1991; Wallevik, 2003)
A_{thix}	1.14	(Roussel & Cussigh, 2008)
λ	Dimensionaless, λ = 1 at full rest, λ → 0 under shear	(ACI Committee 238, 2008)
α	0.001 – 0.01 s	(ACI Committee 238, 2008)
$\dot{\gamma}$	10^{-3} s^{-1} (quasi-static)	(Bischoff & Perry, 1991; Malvar & Ross, 1998)

Table 3. Parameters of 3D Printed Concrete Wall at Fresh State.

Symbol	Typical Value/ Unit	Notes/ References
A_{thix}	0.5–1 Pa/s	Must exceed $\rho gH/\sqrt{3}$ for stability. (Van Der Putten et al., 2019; Wolfs et al., 2018)
$\dot{\gamma}$	1–100 s^{-1}	Higher for faster extrusion or smaller nozzles (Roussel, 2018).
h_0	0.035 m	-
K	10–1,000 Pa·s^n	According to (Roussel, 2018).
n	0.2–0.8 (shear-thinning)	n < 1 for printable concrete. (Roussel, 2018)
S	0.001225 m^2	-
t	2045.33 s	-
v_z	0.0007 m/s	Reported Values in (Le et al., 2012; Van Der Putten et al., 2019) used a delay time (time between layers) usually of 1 seconds, for a layer height of 5 mm. If the Z-movement itself takes 1 second, the instantaneous v_z is 0.7 mm/s (0.0007 m/s).
α_{geom}	$\sqrt{3} \cong 1.73$	According to (Perrot et al., 2016; Wolfs et al., 2018).
μ	30–80 Pa·s	Process-dependent, affects pumpability; lower for easier extrusion (Wolfs et al., 2018).
ρ	2500 Kg/m^3	-
τ_0	10–3,000 Pa	Depends on layer thickness ($\rho g h_0$). Higher for thicker layers (Roussel, 2018).
τ_0 (t)	Up to 30 KPa (for H = 2.5 m)	Must exceed $\rho gH/\sqrt{3}$ to prevent collapse.

Numerical Evaluation for RSCW

At Fresh State

The fresh concrete demonstrates a highly developed internal structure after rest, characterized by a high structural parameter (λ = 2.72). This results in a substantially augmented apparent yield stress of 3532 Pa, as delineated by the governing relationship depicted in Equation (2). The salient feature of this material is its remarkably high flocculation rate of 1.14 Pa/s. This high rate, as indicated by Equation (1), signifies that the concrete undergoes a rapid transition from a fluid to a rigid state.

This phenomenon is advantageous for vertical formwork pressure because the rapid structural build-up reduces lateral pressure swiftly, thereby enabling the concrete to become self-supporting more rapidly. However, this trait presents a significant challenge when it comes to multi-layer placement. According to Equation (3), the critical time window for effective bonding between layers is inversely proportional to the flocculation rate. The elevated rate of 1.14 Pa/s signifies a remarkably constrained operational range. Exceeding this time results in a significant yield stress difference between layers, impeding effective remixing and resulting in a weak plane, known as a cold joint.

At Hardened States

The measured shear stress values (approximately 1200 Pa and 1201 Pa) are interpreted as being near or at the material's yield stress (τ0), consistent with the Bingham model where the shear rate is zero ($\dot{\boldsymbol{\gamma}}$= 0) for stresses below the yield stress (τ < τ0). This phenomenon is indicative of a deformable solid state. The observation of nearly identical stress values indicates a state of impending yield, wherein the application of stress results in elastic deformation without continuous viscous flow. The relatively low power dissipation (P = 3.60 W/m3) is a direct quantitative indicator of a very low shear rate ($\dot{\boldsymbol{\gamma}}$), according to the power-stress-shear rate relationship in Equation (5).

This low dissipation value indicates that the sample was operating within a transition zone, suggesting a phase shift from a viscoplastic solid to a flowing fluid. The power value serves as a critical metric in confirming the limited extent of viscous deformation.

Numerical Evaluation for 3DPW

At Fresh State

As illustrated in Figure 3, the experimental data from the extant literature demonstrate a linear relationship between the yield stress and the duration of rest, thereby validating the seventh equation. The material commences with an almost zero initial yield stress, $\tau_0(0) \approx 0$ Pa, signifying a state of complete fluidization following shearing. The structuration rate, defined as $A_{thix} = 0.75$ Pa/s (Roussel, 2018; Wolfs et al., 2018), represents the rate at which the material rebuilds its internal structure. Subsequent to $t = 1000\ s$, the predicted stress recovery, designated as Δτ₀, exhibited a correspondence with the experimental data. This recovery was determined to be $\Delta\tau_0 = 0.75 \times 1000 = 750$ Pa, thus validating the model's predictions concerning reversible thixotropy. This relationship directly governs printability, as sufficient waiting time between layers ensures that the stress from a new layer does not exceed the increased yield strength of those beneath, thereby maintaining structural stability.

As illustrated in Figure 4, numerical modeling based on Equations (8) and (9) demonstrates the impact of density (ρ) on the printing velocity parameters. As the density of a material increases, the maximum nozzle velocity v_b decreases. This decrease is due to the fact that a heavier material imposes greater self-weight stress, which is proportional to the material's density $\sigma_{grav} \propto \rho\, g\, h_0$. In order to maintain equilibrium, the printing process slows down in one of two ways. The first way is through the lowering of v_b, which results in a reduction of the vertical build rate, $\dot{H}$. It has been demonstrated that the relationship between $v_b$and $\dot{H}$ is satisfied.

Illustrating that any reduction in $v_b$proportionally decreases $\dot{H}$. This adjustment, described by Eq. (8), increases rest time t, allowing more strength gain through $\tau_0(t) = A_{thix}\, t$. Hence, Figures 4(a) and 4(b) demonstrate how printing kinematics and rheological structuration must act synchronously to ensure continuous yet stable layer stacking. Figures 5(a, b), interpreted through Equation (13), show the critical crushing height $H_{c,e}$ as a function of time and density. According to Eq. (14) and Eq. (15) the structure remains stable as long as $\sigma_c(t) > \sigma_v(t)$. As time increases, $\tau_0(t)$ and hence σ_c increase, allowing the printed element to reach a greater height before crushing. Conversely, higher density intensifies gravitational stress, reducing $H_{c,e}$. Thus, light mixtures with sufficient thixotropic growth offer better height capability during printing.

As illustrated in Figure 6, which is based on Equation (17), the critical buckling height, designated as $H_{c,f}$, exhibits a decreasing trend as the density, denoted by ρ, increases. It has been established that the ratio of $E(t)I/(\rho g S)$ is a critical factor in determining buckling stability. An increase in density has been shown to result in an increase in self-weight and a concomitant decrease in the maximum printable height. Therefore, it is imperative to minimize ρand maximize both stiffness E(t) and geometric inertia I to prevent buckling failure. It is imperative that the printing speed be kept in constant alignment with the structuration rate, A_{thix}, throughout the duration of the build process to ensure uninterrupted continuity.

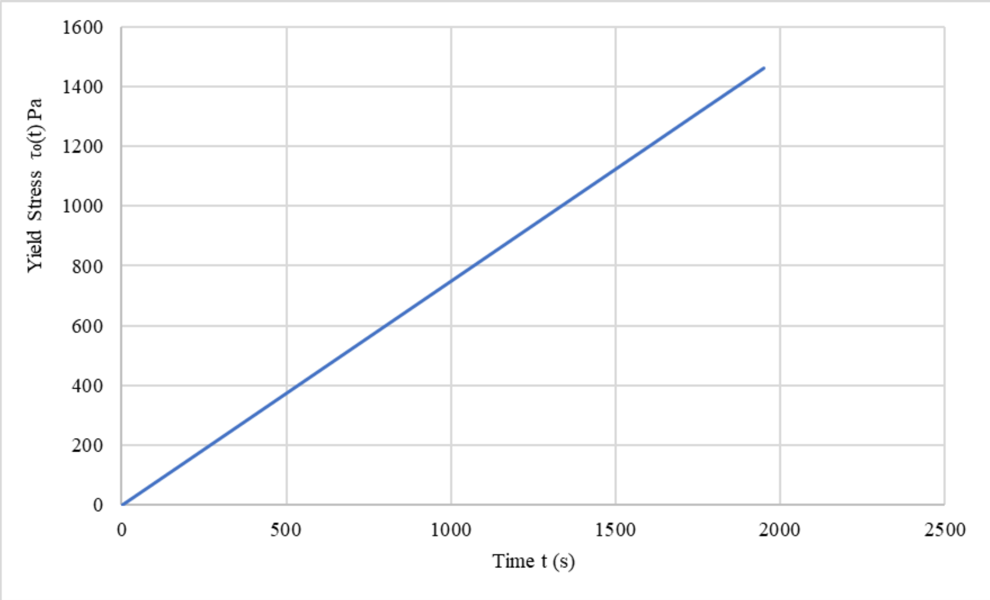

Figure 3. Structuration Kinetics Determined from Yield Stress.

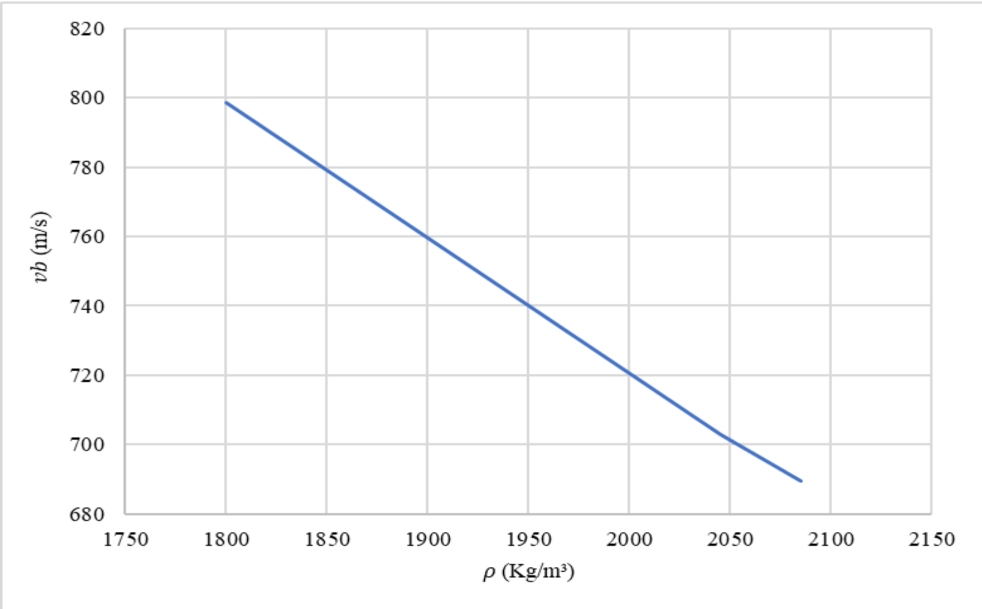

(a)

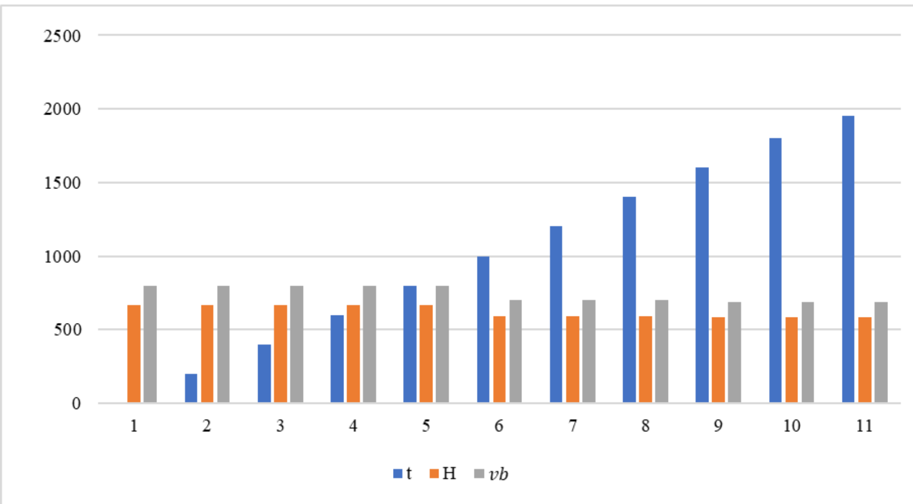

(b)

Figure 4. (a) Material Property Measurements (b) Time-Dependent Evolution of Height and Velocity.

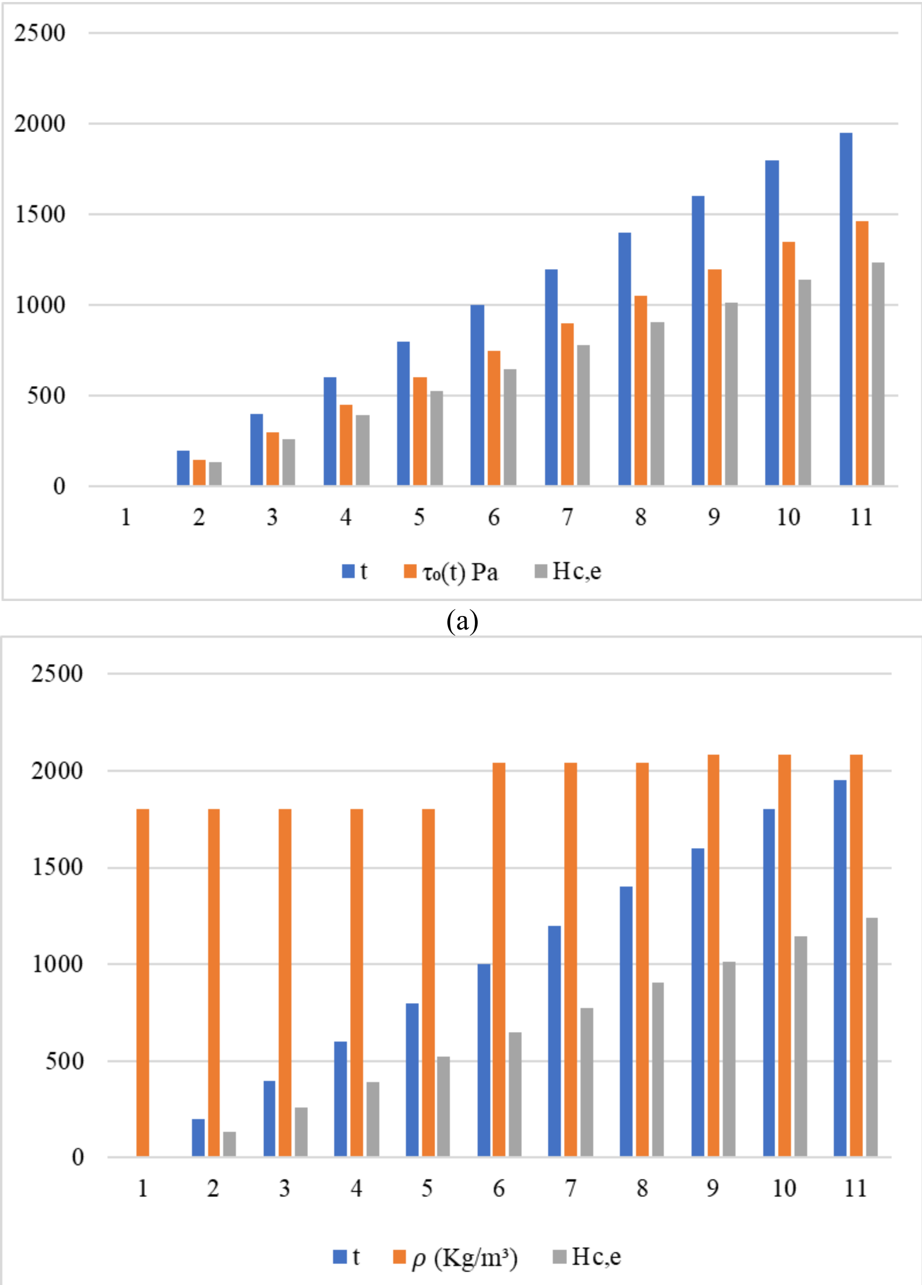

(b)

Figure 5. Time-dependent Evolution of (a) Yield Stress and Critical Height, and (b) Density and Critical Height.

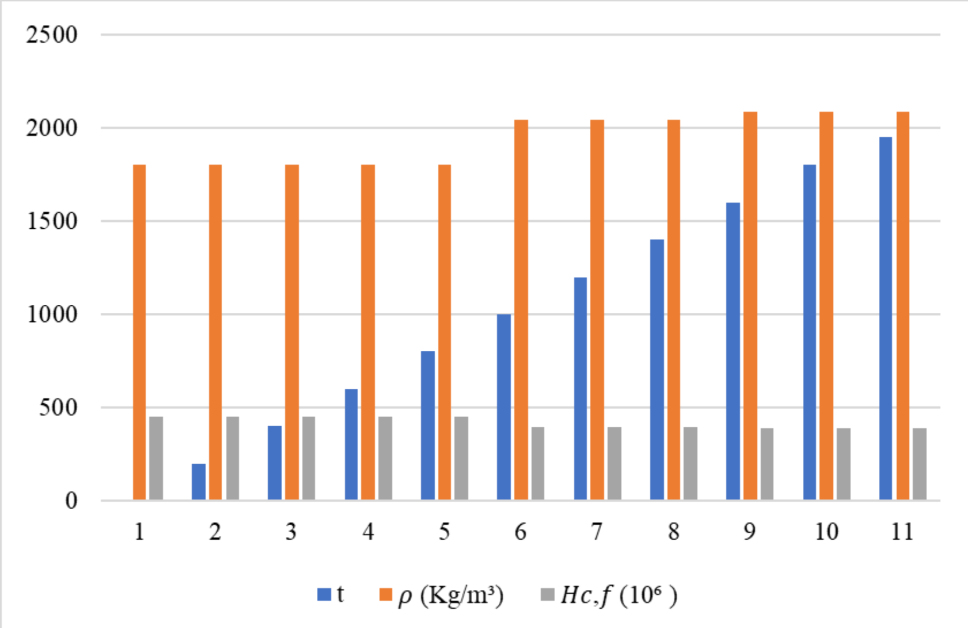

Figure 6. Correlation Between Density and Critical Height $H_{c,f}$ Over Time.

At Hardened State

Two rheological models Herschel–Bulkley (Eq. 11) and Bingham (Eq. 12) were applied to describe shear behavior. The calculated stresses were $\tau = 3570.89$ Pa for Herschel–Bulkley and $\tau = 2750$ Pa for Bingham, differing by about 30%. The Bingham model assumes a linear relationship $\tau = \tau_0 + \mu_p\,\dot{\gamma}$, capturing only simple viscoplastic flow. Conversely, the Herschel–Bulkley model introduces a flow index $n < 1$ to represent shear-thinning, giving $\tau = \tau_0 + K\dot{\gamma}^n$, which aligns more closely with the real behavior of printable concrete. The higher τ value from this model reflects the additional energy required to overcome structural buildup and internal flocculation before steady flow begins. Thus, the Herschel–Bulkley model better predicts the nonlinear, rate-dependent viscosity of 3D printed concrete, balancing buildability and extrudability. The findings confirm that nonlinearity caused by thixotropy, hydration, and particle interaction governs the flow resistance and stability of printed layers making Equation (11) a more realistic rheological descriptor than Equation (12).

Comparative and Discussion

The fundamental divergence between the reinforced shear wall (RSCW) and the 3D printed concrete wall (3DPCW) is rooted in their distinct rheological control mechanisms. Quantitatively, the structuration rate A_{thix} of the RSCW mix employed in this simulation is 1.14 Pa/s, which is approximately 52% higher than the 0.75 Pa/s observed in the 3DPCW mix. From an engineering perspective, this higher rate in RSCW accelerates the transition to a self-supporting state, thereby effectively reducing lateral formwork pressure.

However, this rapid build-up significantly compromises the "interlayer bonding window." As demonstrated in Equation (3), the RSCW's high flocculation rate signifies a heightened risk of "cold joints," where a delay in casting results in a 3532 Pa yield stress barrier that hinders the microscopic remixing of subsequent layers. In contrast, the 3DPCW relies entirely on its time-dependent evolution to maintain structural integrity without external support. A numerical sensitivity analysis was conducted on the 3DPCW system, revealing a high degree of dependence on material density (ρ). When the density was increased from 2085 to 2500 kg/m³ (a 20% increase), it was necessary to reduce the permissible nozzle velocity v_b by approximately 15% to maintain dynamic equilibrium (Equation 8). The quantitative correlation indicates that, in the context of 3D printing, every increase in self-weight must be counterbalanced by a proportional decrease in the vertical build rate $\dot{H}$. This adjustment enables the yield stress τ0 (t) to adequately respond to the increasing gravitational stresses. A thorough comparison of the failure thresholds reveals the presence of two distinct stability regimes. For the 3DPCW, the critical crushing height, designated as Hc,e, exhibited a substantial time-dependency, increasing from 0.4m at 400s to 1.2m at 1200s.

In the RSCW, the material remains confined by formwork, meaning its "critical height" is effectively infinite until the formwork is removed. However, the 3DPCW's stability is further constrained by buckling (Equation 17), where the stiffness-to-weight ratio becomes the governing factor. Quantitatively, the non-linear Herschel-Bulkley model yielded a 30% higher stress prediction (3570 Pa) than the linear Bingham model (2750 Pa), with a flow index of n≈ 0.5. The observed 30% discrepancy serves to substantiate the assertion that the observed shear-thinning behavior is not merely a theoretical observation but rather a quantitative necessity for 3DPCW, thereby ensuring high extrudability while maintaining shape retention post-deposition.

The data indicates that optimal printing stability is attained only when the ratio of A_{thix} exceeds 1 s/m and the density remains below 2200 kg/m³. These quantitative benchmarks establish a clear engineering envelope: while RSCW design emphasizes the management of "cold joints," 3DPCW design must prioritize the synchronization of printing kinematics with rheological growth to avert catastrophic structural collapse.

Conclusion

The present study established a cohesive rheological-mechanical framework to compare the early-age structural stability of Reinforced Shear Concrete Walls (RSCW) and 3D-Printed Concrete Walls (3DPW). The following specific conclusions are drawn:

- The RSCW system demonstrates a high structuration rate (A_{thix}= 1.14 Pa/s), which is 52% higher than that of the 3DPCW mix (0.75 Pa/s). While this facilitates a rapid reduction in lateral formwork pressure, it creates a high yield stress barrier (3,532 Pa) that significantly narrows the interlayer bonding window, increasing "cold joint" risks.
- The 3DPCW model differs from the formwork-confined RSCW model in that it is governed by a time-dependent critical crushing height (Hc,e) that evolves from 0.4 m at 400 s to 1.2 m at 1200 s. Numerical analysis identifies a 30% discrepancy between the Bingham and Herschel-Bulkley models, confirming that a flow index of n ≈ 0.5 is a quantitative necessity for predicting the non-linear stability of printed layers.
- A critical sensitivity exists between material density and printing speed. A 20% increase in density (ρ) necessitates a 15% reduction in nozzle velocity (v_b) to maintain structural equilibrium. The stability of the deposition process is constrained by two key parameters: the $A_{thix}/\dot{H}$ ratio, which must exceed 1 s/m, and a density threshold of less than 2,200 kg/m³.

The novelty of this research lies in the direct quantitative bridging of traditional viscoplastic models with the kinematic requirements of additive manufacturing. This work proposes a unified model that conceptualizes concrete as a transitionary material, undergoing a phase transition from a fluidized state to a self-supporting solid without external containment. The model provides specific "safe printing envelopes" that optimize the synchrony between the mechanical strength gain and robotic deposition speeds. While this numerical study provides a robust parametric baseline, it is limited by the assumption of linear yield stress evolution over short time scales. The present model does not fully account for the thermal hydration effects on stiffness (E(t)) or the stochastic nature of interlayer porosity in printed elements. In the future, researchers should consider integrating thermo-chemical coupling with large-scale experimental buckling tests. This integration could lead to significant advancements in the predictive accuracy of the proposed buckling height equations (Hc,f).

Declarations

Authors' Contributions

S.A.M: Conceptualization, Methodology, Validation, Formal analysis, Investigation, Data curation, Writing of the original draft.

H.AA: Conceptualization, Methodology, Validation, Supervision, Writing – review & editing.

Conflict of Interest

The authors declare that they have no known competing financial interests or personal relationships that could have appeared to influence the work reported in this paper.

Funding

This research did not receive any specific grant from funding agencies in the public, commercial, or not-for-profit sectors.

Declaration on the Use of Generative AI and AI-Assisted Technologies

The author(s) utilized ChatGPT (OpenAI) for linguistic assistance in restructuring and refining sentences following manual summarization of source materials (Not used in abstract, methodology, conclusion). All AI-generated text was carefully reviewed, fact-checked, and revised by the author(s) to ensure accuracy and alignment with the intended meaning. The final manuscript remains the sole intellectual responsibility of the author(s)..

Data Availability

The data that support the findings of this study are available from the corresponding author upon reasonable request.

Acknowledgement

The authors declare that there is no acknowledgement to be made.

Ethics

This study did not involve human participants or animals; hence, no ethical approval was required.

References

ACI Committee 238. (2008). *Report on measurements of workability and rheology of fresh concrete (ACI 238.1R-08)*. American Concrete Institute.

ACI Committee 318. (2014). *Building Code Requirements for Structural Concrete (ACI 318-14) [and] Commentary on Building Code Requirements for Structural Concrete (ACI 318R-14)*. American Concrete Institute.

Banfill, P. F. G. (1991). *Rheology of Fresh Cement and Concrete* (P. F. G. BANFILL, Ed.). Taylor & Francis. https://doi.org/10.4324/9780203473290

Benamara, A. (2021). *Impression 3D de matériaux dédiés à la construction : De la définition des encres, maîtrise de l'impression à la performance des produits imprimés*. Cergy-Pontoise University, Français.

Bischoff, P. H., & Perry, S. H. (1991). Compressive behaviour of concrete at high strain rates. *Materials and Structures*, *24*(6), 425–450. https://doi.org/10.1007/BF02472016

Bos, F., Wolfs, R., Ahmed, Z., & Salet, T. (2016). Additive manufacturing of concrete in construction: potentials and challenges of 3D concrete printing. *Virtual and Physical Prototyping*, *11*(3), 209–225. https://doi.org/10.1080/17452759.2016.1209867

Buchanan, C., & Gardner, L. (2019). Metal 3D printing in construction: A review of methods, research, applications, opportunities and challenges. *Engineering Structures*, *180*, 332–348. https://doi.org/10.1016/j.engstruct.2018.11.045

Ferraris, C. F. (1999). Measurement of the rheological properties of high performance concrete: State of the art report. *Journal of Research of the National Institute of Standards and Technology*, *104*(5), 461. https://doi.org/10.6028/jres.104.028

Hernández Vargas, J. (2023). *Design for 3D Concrete Printing: Optimisation Through Integrated Workflows* [KTH Royal Institute of Technology]. https://doi.org/10.13140/RG.2.2.17781.18409

ISO/ASTM 52900:2021(en). (2021). *Additive manufacturing — General principles — Fundamentals and vocabulary*. https://www.iso.org/obp/ui/#iso:std:iso-astm:52900:ed-2:v1:en

Khoshnevis, B. (2004). Automated construction by contour crafting—related robotics and information technologies. *Automation in Construction*, *13*(1), 5–19. https://doi.org/10.1016/j.autcon.2003.08.012

Kosmatka, S. H. ., & Wilson, M. L. . (2011). *Design and control of concrete mixtures : the guide to applications, methods, and materials*. Portland Cement Association.

Kruger, J., Zeranka, S., & van Zijl, G. (2019). 3D concrete printing: A lower bound analytical model for buildability performance quantification. *Automation in Construction*, *106*, 102904. https://doi.org/10.1016/j.autcon.2019.102904

Le, T. T., Austin, S. A., Lim, S., Buswell, R. A., Gibb, A. G. F., & Thorpe, T. (2012). Mix design and fresh properties for high-performance printing concrete. *Materials and Structures*, *45*(8), 1221–1232. https://doi.org/10.1617/s11527-012-9828-z

Le, T. T., Austin, S. A., Lim, S., Buswell, R. A., Law, R., Gibb, A. G. F., & Thorpe, T. (2012). Hardened properties of high-performance printing concrete. *Cement and Concrete Research*, *42*(3), 558–566. https://doi.org/10.1016/j.cemconres.2011.12.003

Ma, G., Li, Z., & Wang, L. (2018). Printable properties of cementitious material containing copper tailings for extrusion based 3D printing. *Construction and Building Materials*, *162*, 613–627. https://doi.org/10.1016/j.conbuildmat.2017.12.051

Malvar, L. J., & Ross, C. A. (1998). Review of Strain Rate Effects for Concrete in Tension. *ACI Materials Journal*, *95*(6), 735–739. https://doi.org/10.14359/418

Masonry Standards Joint Committee. (2013). *Building code requirements and specification for masonry structures : containing Building code requirements for masonry structures (TMS 402-13/ACI 530-13*. Masonry Society ; American Concrete Institute ; Structural Engineering Institute of the American Society of Civil Engineers.

Mechtcherine, V., Nerella, V. N., Will, F., Näther, M., Otto, J., & Krause, M. (2019). Large-scale digital concrete construction – CONPrint3D concept for on-site, monolithic 3D-printing. *Automation in Construction*, *107*, 102933. https://doi.org/10.1016/j.autcon.2019.102933

Mehta, P. Kumar., & Monteiro, P. J. M. . (2014). *Concrete : microstructure, properties, and materials* (4th ed.). McGraw-Hill Education.

Mindess, Sidney., Young, J. Francis., & Darwin, David. (2003). *Concrete*. Prentice Hall.

Neville, A. . (2012). *Properties of Concrete, Fifth Edition*. Prentice Hall.

Panda, Biranchi., Shakor, P. N. ., & Laghi, Vittoria. (2024). *Additive manufacturing for construction*. Emerald Publishing Limited : ICE Publishing, an imprint of Emerald Publishing Limited.

Perrot, A., Rangeard, D., & Pierre, A. (2016). Structural built-up of cement-based materials used for

3D-printing extrusion techniques. *Materials and Structures*, *49*(4), 1213–1220. https://doi.org/10.1617/s11527-015-0571-0

Roussel, N. (2006). A thixotropy model for fresh fluid concretes: Theory, validation and applications. *Cement and Concrete Research*, *36*(10), 1797–1806. https://doi.org/10.1016/j.cemconres.2006.05.025

Roussel, N. (2018). Rheological requirements for printable concretes. *Cement and Concrete Research*, *112*, 76–85. https://doi.org/10.1016/j.cemconres.2018.04.005

Roussel, N., & Cussigh, F. (2008). Distinct-layer casting of SCC: The mechanical consequences of thixotropy. *Cement and Concrete Research*, *38*(5), 624–632. https://doi.org/10.1016/j.cemconres.2007.09.023

Tattersall, G. H. ., & Banfill, P. F. G. . (1983). *The rheology of fresh concrete*. Pitman Advanced Pub. Program.

Van Der Putten, J., De Schutter, G., & Van Tittelboom, K. (2019). The effect of print parameters on the (micro)structure of 3D printed cementitious materials. *First RILEM International Conference on Concrete and Digital Fabrication – Digital Concrete 2018*, *19*, 234–244. https://doi.org/10.1007/978-3-319-99519-9_22

Wallevik, O. (2003). Rheology - A scientific approach to develop self-compacting concrete. *Proceedings of the 3rd International RILEM Symposium on Self-Compacting Concrete*, 23–31.

Wolfs, R. J. M., Bos, F. P., & Salet, T. A. M. (2018). Early age mechanical behaviour of 3D printed concrete: Numerical modelling and experimental testing. *Cement and Concrete Research*, *106*, 103–116. https://doi.org/10.1016/j.cemconres.2018.02.001

Wolfs, R. J. M., Bos, F. P., & Salet, T. A. M. (2019). Hardened properties of 3D printed concrete: The influence of process parameters on interlayer adhesion. *Cement and Concrete Research*, *119*, 132–140. https://doi.org/10.1016/j.cemconres.2019.02.017